

# A Surprisingly Simple Electrostatic Model Explains Bent vs. Linear Structures in $M^+-RG_2$ species

(M = Group 1 Metal, Li–Fr; RG = Rare Gas, He–Rn)

Anna Andrejeva<sup>a</sup>, W. H. Breckenridge<sup>b</sup> and Timothy G. Wright<sup>a\*</sup>

<sup>a</sup>School of Chemistry, University of Nottingham, University Park, Nottingham, NG7 2RD, U.K.

<sup>b</sup>Department of Chemistry, University of Utah, Salt Lake City, Utah, 84112, USA

\*To whom correspondence should be addressed. Email: [Tim.Wright@nottingham.ac.uk](mailto:Tim.Wright@nottingham.ac.uk)

A Surprisingly Simple Electrostatic Model Explains Bent vs. Linear  
Structures in  $M^+-RG_2$  species

(M = Group 1 Metal, Li–Fr; RG = Rare Gas, He–Rn)

## ABSTRACT

It is found that a simple electrostatic model involving competition between the attractive dispersive interaction and induced-dipole repulsion between the two RG atoms performs extremely well in rationalizing the  $M^+-RG_2$  geometries, where  $M$  = Group 1 metal and RG = rare gas. The  $Li^+-RG_2$  and  $Na^+-RG_2$  complexes have previously been found to exhibit quasilinear or linear minimum energy geometries, with the  $Na^+-RG_2$  complexes having an additional bent local minimum [A. Andrejeva, A. M. Gardner, J. B. Graneek, R. J. Plowright, W. H. Breckenridge and T. G. Wright, *J. Phys. Chem. A*, 2013, **117**, 13578]. In the present work, the geometries for  $M = K-Fr$  are found to be bent. A simple electrostatic model explains these conclusions and is able to account almost quantitatively for the binding energy of the second RG atom, as well as the form of the angular potential, for all thirty six titular species. Additionally, results of population analyses are presented together with orbital contour plots; combined with the success of the electrostatic model, the expectation that these complexes are all physically bound is confirmed.

## 1. INTRODUCTION

Pairwise potentials are prevalent in determining the structures of large aggregates of atoms and molecules. The pairwise potentials are often calculated using quantum chemical calculations (perhaps evaluated against any available experimental data), and then applied to larger systems, which are computationally prohibitive for quantum chemistry methods. Simple Lennard-Jones type potentials are also popular, with parameters often determined via fitting to higher-quality quantum chemistry results or to experiment. For neutral species, the limitations of pairwise potentials have recently been reviewed<sup>1</sup> and workers have included three-body terms to obtain a more realistic representation of the interactions in such complexes – see, for example, refs. 2, 3 and work cited therein. Such treatments can be somewhat involved and uncertain. Here, we shall show that the addition of a single term to the pairwise model for simple  $M^+$ -RG<sub>2</sub> systems gives results that are in surprisingly good agreement with our quantum-chemical results over a wide range of angles for all thirty six titular species.

Metal cation/ligand complexes are prototypes for a wide range of chemical and biochemical phenomena. Detailed consideration of the latter is often difficult, and hence studies on isolated complexes are used to build up a picture of how cumulative solvation is able to affect the physical and chemical properties of the cation, with rare gas (RG) atoms being the simplest such ligand. A large proportion of previous experimental and theoretical studies (see ref. 4 and references therein) have concentrated on a single metal cation interacting with a single rare gas (RG) atom,  $M^+$ -RG. In previous work, we have extended the work in ref. 4 and studied a number of these complexes ourselves including both alkali<sup>5,6</sup> and alkaline earth metals.<sup>7,8,9</sup> It was shown for Group 1 complexes that interactions remain purely physical in nature, a fact reflected in their relatively low binding energies. In contrast, the Group 2 species showed significantly higher dissociation energies compared to their Group 1 counterparts, and this has been attributed to hybridization between the outer s orbital on the metal cation and the lowest unoccupied p or d orbital.<sup>10</sup> This occurs as the RG atom approaches the metal center and leads to electron density being able to move away from the incoming RG atom, reducing electron repulsion; concomitantly, this movement of electron density leads to a greater exposure of the dicationic metal core, and so increasing attractive terms.

Larger complexes provide a bridge between a single molecular or atomic ion in the gas phase, and bulk material. These have also been studied in abundance in the past decade, where noble gas clusters doped with a metal ion have attracted significant interest.<sup>11,12</sup> Just as Group 1 and 2 diatomic  $M^+$ -RG species remain some of the most-studied species, higher-order complexes of the form  $M^+$ -RG<sub>n</sub> (M = alkali metal) have been studied both theoretically and experimentally. Most of such studies have concentrated on M = Li and Na,<sup>13,14,15,16</sup> but studies have also been performed on Group 2  $M^+$ -RG<sub>n</sub> clusters<sup>17,18,19</sup> where n can range from 1 up to 25. In these studies, the emphasis is usually placed on the higher values of n. It is also worth noting that the majority of these studies adopt pairwise potentials and, as is well known, such models will be missing key electrostatic terms and, as will be discussed, this can affect conclusions on geometric structure.

A study by Bauschlicher et al.<sup>20</sup> was one of the first to look at  $M^+-RG_2$  complexes, whose study was focused on  $RG = Ar$  with different  $M^+$  ions,  $M = Li, Na, Mg, V, Ni$  and  $Cu$ . Since that work, only a few studies have been reported in which  $M^+-RG_2$  species have been the focus of study; as an example, the  $Na^+-Ar_2$  complex has been concluded to be linear employing model potentials, including three-body terms, although the emphasis was on growth mechanisms for larger complexes.<sup>16</sup> To the best of our knowledge there have been no studies where geometric trends or spectroscopic constants for a whole series of  $M^+-RG_2$  complexes have been studied and rationalized for a particular elemental group.

We have shown in our previous work on the  $Li^+-RG_2$  and  $Na^+-RG_2$  complexes,<sup>21</sup> that these species have very flat angular potentials, and exhibit quasilinear or linear minimum energy geometries. Group 2  $M^+-RG_2$  complexes for  $M = Be$  and  $Mg$ , however, were found<sup>21</sup> to be of  $C_{2v}$  symmetry with bent minimum geometries. The latter was attributed to  $sp$  hybridisation of the outer  $s$  orbital on the metal center with the lowest unoccupied  $p$  orbital, making it favourable for the second  $RG$  atom to approach  $M^+$  from the same side; such hybridization is not possible for the Group 1 metals, as the unoccupied orbitals are too high in energy. However, in the present work we shall conclude that the  $M^+-RG_2$  complexes involving the heavier alkali metals are bent, and thus there is a need to rationalize this in contrast to the linear lighter species.

As far as we have been able to ascertain, the only previous study on the heavier  $M^+-RG_2$  ( $M = K-Fr$ ) complexes is by Hernández-Rojas and Wales,<sup>17</sup> where the authors present candidate structures for the global minima points for the  $n$ -atom rare gas clusters containing  $K^+$  and  $Cs^+$  metal cations ( $n = 1-79$ ). Their work, which involved model pairwise potentials rather than quantum chemistry calculations, showed that the  $K^+-Ar_2$  and  $Cs^+-Xe_2$  species had  $C_{2v}$  global minimum geometries; no rationalization of these geometries was presented in ref. 17 since the emphasis was on the larger complexes. These bent structures are, of course, in contrast to the (quasi)linear structures we<sup>21</sup> and others<sup>16,20</sup> have reported for the lighter species ( $M = Li$  and  $Na$ ). In the present work, we complete the overall study of alkali metal  $M^+-RG_2$  complexes by reporting the results on the remaining twenty four systems involving  $M = K-Fr$  and  $RG = He-Rn$ . We find that all of these heavier complexes have a bent global minimum. We propose a simple rationalization of the bent and linear geometries found for the complete set of thirty six  $M^+-RG_2$  complexes in terms of a simple electrostatic model.

## 2. COMPUTATIONAL DETAILS

Geometry optimizations and harmonic vibrational frequency calculations of the  $M^+-RG_2$  species ( $M = K, Rb, Cs$  and  $Fr$ ; and  $RG =$  rare gas,  $He-Rn$ ) were performed using the MP2 method, employing the quintuple- $\zeta$  quality basis sets described below. Linear and bent geometries were considered as starting points during the optimization process where “tight” energy and gradient criteria were employed in order to obtain reliable optimized global minimum structures. Additionally, angular scans were performed, where at each fixed angle the internuclear distances were independently optimized in order to yield a minimum energy path along the angular coordinate.

A quintuple- $\zeta$  valence basis set for  $K^+$ , equivalent to aug-cc-pV5Z (no h functions) quality, (described fully in Ref. 22) is used here with the small-core quasirelativistic effective core potential, ECP10MWB.<sup>23</sup> For  $Rb^+$ ,  $Cs^+$  and  $Fr^+$ , ECP28MWB,<sup>23</sup> ECP60MWB<sup>23</sup> and ECP78MWB<sup>24</sup> quasirelativistic effective core potentials were used, respectively; the valence basis sets for these metals are described in detail in ref. 25 and are of the same quality as the  $K^+$  basis set.

For He and Ne, standard aug-cc-pV5Z basis sets<sup>26,27</sup> were utilized, whereas Ar utilized the standard aug-cc-pCV5Z basis set.<sup>28</sup> For the heavier rare gases, Kr, Xe and Rn, ECP28MWB, ECP46MWB and ECP78MWB quasirelativistic effective core potentials<sup>29,30</sup> were employed, respectively, along with the corresponding aug-cc-pwCV5Z-PP valence basis sets.<sup>31</sup> None of the rare gas basis sets included h or higher orbital angular momentum functions, consistent with the basis sets used for the metal species. These combinations of basis sets are simply referred to as aV5Z in the below.

In the MP2 method, the valence electrons of He–Ar were correlated, while for Kr, Xe and Rn all of the electrons not described by the ECP were correlated. All of the above calculations employed the MOLPRO suite of programs.<sup>32</sup> In calculating dissociation energies, the counterpoise correction was not employed since we are using a quintuple- $\zeta$  basis set where such basis set superposition errors are expected to be small; further, this would have been difficult to apply consistently through the range of calculations performed.

Three population analyses were undertaken: natural population analysis (NPA),<sup>33</sup> atoms-in-molecules (AIM)<sup>34</sup> and Mulliken.<sup>35</sup> The AIM analyses utilised the AIMAll software package<sup>36</sup> using WFX files produced by Gaussian09.<sup>37</sup> NPA analyses were performed using the NBO 6.0<sup>38</sup> software package and Mulliken analysis was used as implemented in Gaussian09. The calculations were performed with the MP2/aV5Z natural orbital density at the corresponding optimized geometries.

### 3. RESULTS AND DISCUSSION

#### A. Geometries

Table 1 shows the results of the geometry optimizations, where it can be seen that the entire set of the heavier  $M^+$ -RG<sub>2</sub> species ( $M = K, Rb, Cs$  and  $Fr$ ; and RG = rare gas, He–Rn) exhibit bent minimum geometries. Harmonic vibrational frequencies were calculated to confirm the nature of the stationary points found and these are presented in Table 2; three real frequencies were obtained in each case. The values are all quite small, with tight convergence criteria needing to be used during the optimization and small step sizes needed for the numerical second derivative procedures in order to obtain all real vibrational frequencies. The low values obtained means that these values can only be taken as indicative, as the true anharmonic values are likely to be significantly different. Even so, we can see from the magnitude of the bending modes that the very shallow minima for some of the complexes means a number of these could be quasilinear (i.e. floppy) once zero-point vibrational energy is included.

Optimized internuclear separations between the metal cation and the rare gas atoms for the heavier alkali metals for both  $M^+-RG_2$  (denoted  $R_{e2}$ ) and  $M^+-RG$  (denoted  $R_{e1}$ ) complexes are given in Table 1, with the optimized geometries of the lighter species reported in ref. 21. Note that in Table 1, the  $R_{e1}$  values have been obtained in the present work from optimizations using the same MP2/aV5Z method as used for the  $M^+-RG_2$  complexes. In all of the  $M^+-RG_2$  species studied, it was found that the  $M^+-RG$  equilibrium separations are equal, i.e. the symmetry is  $C_{2v}$ . It may also be seen that the equilibrium separations in the  $M^+-RG_2$  and  $M^+-RG$  species are almost identical, suggesting that a dominant driving force for the interaction is achieving internuclear  $M^+...RG$  separations that are close to the optimal values in the diatomic  $M^+-RG$  complexes; consequently,  $R_{e2}/R_{e1}$  ratios are seen to be very close to 1.00 for these complexes (Table 1). As expected, these values increase monotonically as the atomic number of RG increases, as was noted in ref. 5 for the  $R_{e1}$  trends. The trend is rationalized by the increasing attraction caused by the rise in the polarizabilities of the RG atom with atomic number,<sup>39</sup> which outweighs the concomitant increasing size. Additionally, for a fixed RG, the  $D_e$  values fall monotonically with increasing atomic number of the metal cation in line with the increasing internuclear separations – this clearly outweighs the increasing polarizability of the cation.

It may also be seen in Table 1 that the  $RG-M^+-RG$  angle increases monotonically with increasing atomic number of the RG atom, which is in line with the increasing size of RG. A hint as to why a bent geometry is preferred to a linear one for the  $M^+-RG_2$  complexes ( $M = K-Fr$ ) can be found by considering the internuclear separation between two RG atoms at the minimum energy geometry of the complex with the equilibrium value of the  $RG_2$  dimer,  $R_e(RG_2)$ . The latter values have been obtained at the same level of theory and using identical basis sets as employed for the  $M^+-RG_2$  calculations. It was found that in all of the species studied, the  $R_{RG-RG}$  values were slightly larger than the  $R_e(RG_2)$  values. This is consistent with simple electrostatics arguments which will be considered shortly; however, first we examine the atomic charges.

## **B. Atomic Charges and Contour Plots**

In Table 3, we present the results of three population analyses for the  $M^+-RG_2$  complexes: Mulliken, NPA and AIM. There is agreement between the AIM and NPA methods that there is very little charge transfer from the metal to the rare gas atoms. In contrast, Mulliken charge analysis gives small, but more significant charge transfer in both  $M^+-RG_2$  and  $M^+-RG$  systems; however, it is well established that Mulliken populations can be unreliable. Both AIM (values in bold in Table 3) and NPA (values in square brackets in Table 3) results are in line with the expected very small charge movement for physical interactions; additionally, these results are consistent with those for the  $Li^+-RG_2$  and  $Na^+-RG_2$  complexes.<sup>21</sup>

The general trend for the values in Table 3 is that there is a very slight decrease in atomic charge on the metal with increasing atomic number of the rare gas atom which is consistent with the increasing polarizability and decreasing ionization energy of the RG atom. The AIM and NPA charges are very close to each other and look reasonable, with essentially all of the charge still being located on the  $M^+$  cation, consistent with previous deductions that the

Group 1 diatomic  $M^+$ -RG complexes are described well by an essentially physical model.<sup>4,40,41</sup> Indications are that only for the heaviest species does a very small amount of charge transfer possibly occur, but even then this is likely within the reliability of the population method. The interactions in the Group 1  $M^+$ -RG and  $M^+$ -RG<sub>2</sub> systems are in contrast to the corresponding Group 2 complexes with their facile sp and sd hybridization, which may be viewed as chemical effects.<sup>7,8,9,21,42</sup> Such hybridization is not possible for the Group 1 complexes, as there are no low-lying p or d orbitals<sup>43</sup> (see Table 4, and comments below).

The AIMAll software package was also used to obtain the total local energy density parameter,  $H(R)$ , which is found by analysis of the electron density at so-called bond critical points, BCPs; for a covalent or other chemical bond, the local energy density  $H(R)$  will always be negative.<sup>44,45,46</sup> Analysis of the  $H(R)$  parameter at the BCPs of both the  $M^+$ -RG<sub>2</sub> and  $M^+$ -RG complexes yielded positive values across the whole series, confirming the above conclusion that there is essentially no chemical bonding character in these systems.

Additionally, the NBO 6.0 program was used to determine natural bonding orbitals (NBOs) by performing the analysis of a many-electron molecular wavefunction in terms of localized electron-pair bonding units. It is well demonstrated in the literature that the method can determine the degree of hybridization successfully in terms of contributions of the atomic functions to the molecular orbitals.<sup>47</sup> No such hybridization was seen for the Group 1  $M^+$ -RG<sub>2</sub> species, in line with expectations noted above.

In Figure 1 we present the Hartree-Fock (HF) contour plots of the highest-occupied molecular orbital (HOMO) for selected  $M^+$ -RG<sub>2</sub> species, which have been calculated at both the global bent minimum and at the linear geometry (which are sometimes local minima) at the MP2/quintuple- $\zeta$  level of theory. The contour spacings employed are the same for all species. (We note that in unpublished work on a number of systems we have compared HF contour plots with those from natural orbitals from correlated calculations, MP2 and QCISD, obtaining excellent agreement, as long as the optimized geometry with the correlated method is employed.) As may be seen, the HOMOs correspond to antibonding combinations of the outermost occupied p orbitals of the RG atoms, or of the 1s orbitals in the case of He. It is also apparent that there is only very little perturbation of the atomic orbitals as a result of the interaction. The little effect that there is may be seen to correspond to a slight compression of the interacting lobes of the p orbitals in the heavier species as a result of the interactions pulling these atoms together. As a consequence, we conclude that the rationale for the bent geometries for the heavier Group 1  $M^+$ -RG<sub>2</sub> species is different to that for the corresponding Group 2 ones.<sup>21</sup>

### **C. Dissociation Energies**

Table 1 contains the calculated dissociation energies for the removal of a single RG atom from the heavier  $M^+$ -RG<sub>2</sub> system,  $D_{e2}$ . These are also compared to the corresponding Group 1  $M^+$ -RG values, denoted  $D_{e1}$ , and we also give the  $D_{e2}/D_{e1}$  ratios. (We note that in refs. 21 and 42, we saw that  $D_e$  values obtained at the MP2 level, using triple- $\zeta$  and quadruple- $\zeta$  basis sets

were within a few percent of those obtained at the RCCSD(T) level using quintuple- $\zeta$  basis sets, giving confidence in the present interaction energies.)  $D_{e2}$  increases monotonically for the  $M^+$ -RG<sub>2</sub> species as the atomic number of the RG atom is increased and these observations are in line with the corresponding  $D_{e1}$  trends. (The same method and basis set were employed for both the  $D_{e1}$  and  $D_{e2}$  calculations.) The increasing polarizability of the RG atoms with atomic number appears to drive the increase in dissociation energies, and outweighs the increasing repulsion terms from the greater number of electrons. For the  $K^+$ -RG<sub>2</sub> complexes, the  $D_{e2}/D_{e1}$  ratios are quite close to unity, but are always greater; additionally, the ratios generally increase with both the atomic number of M and RG, which we shall comment on in subsection (e). Similar results and discussions were presented in ref. 21 for the two lightest Group 1  $M^+$ -RG<sub>2</sub> species.

#### **D. Angular Cuts Through the Potential Energy Surfaces**

Figure 2 shows angular cuts through the  $M^+$ -RG<sub>2</sub> potential energy surfaces for the selected species,  $M = K - Fr$  and  $RG = He, Ar$  and  $Xe$ . Potential energy surface cuts are presented for a range of angles that cover the linear region and bent geometries. In these calculations, the internuclear distances have been independently optimized at each fixed angular coordinate. We reiterate that the MP2 method is able to obtain reliable results for the more challenging  $D_e$  values, and we expect the angular plots to be more reliable since we are not calculating energy differences between fragments, but merely variations in energy with geometry. Figure 2a shows  $M^+$ -He<sub>2</sub> angular plots, with corresponding  $M^+$ -Ar<sub>2</sub> and  $M^+$ -Xe<sub>2</sub> ones presented in Figures 2b and 2c, respectively. In all of these plots, a bent geometry can be seen to correspond to the global minimum, and the same is true for the  $M^+$ -Ne<sub>2</sub>,  $M^+$ -Kr<sub>2</sub> and  $M^+$ -Rn<sub>2</sub> systems (see Table 1). It is interesting that some of the plots appear “wobbly”, particularly for  $RG = He$ : we have checked this carefully, using tighter convergence criteria, and this is genuine. We suspect it arises owing to the small size of He and its sensitivity to the electronic environment, such as the ability for its electrons to access the  $Fr^+$  virtual orbitals (albeit to a very limited extent) – angular plots were presented in ref. 21 for the two lightest Group 1  $M^+$ -RG<sub>2</sub> species.

For the  $M^+$ -RG<sub>2</sub> ( $M = K-Fr$ ) complexes, energy differences between the linear structures and the bent minima were calculated and these are presented in Table 5 (note that for  $M = Li$  and  $Na$ , the equilibrium structures were linear or quasilinear and so we do not include the energy differences for these). There can be seen to be a general increase in the bent-linear energy difference for a fixed RG when moving through the  $M = K - Fr$  species. Additionally, for a particular M, there is also such an increasing trend with atomic number of the RG atom, with the smallest energy difference for the He-containing species and largest ones for the Rn-containing complexes. Some of these energy differences suggest that the species will be quasilinear; for example, for the  $K^+$ -He<sub>2</sub> and  $Rb^+$ -He<sub>2</sub> species the values are only  $\sim 2-3$  cm<sup>-1</sup>, suggesting that even with zero-point vibrational energy, the complex can sample a wide range of angles on the very flat potential energy surface. In contrast, for other complexes, such as  $Cs^+$ -Xe<sub>2</sub>, the energy difference rises to over 175 cm<sup>-1</sup>, which suggests that this will be a truly bent structure. The linear minima for  $Li^+$ -RG<sub>2</sub> and  $Na^+$ -RG<sub>2</sub> species were also very shallow even for heavier RGs and so these structures were concluded to be quasilinear.<sup>21</sup>

## **E. Simple Electrostatic Model**

We now consider a simple electrostatic model which is found to replicate, surprisingly well, the observed linear and bent geometries, and even more quantitative aspects of the Group 1  $M^+RG_2$  potential energy surfaces. As we shall note below, there are more complicated versions of this model, but we shall conclude that a simple model suffices to explain the geometries of the whole set of thirty six  $M^+RG_2$  complexes.

### *(i) “Zeroth-Order” Pairwise Model*

We commence by considering a simple pairwise interaction potential. In this case, the RG atoms will move into a position whereby they maximize their interaction with both the  $M^+$  ion and also each other, independently. That is, they will take up a bent geometry of necessity, where the internuclear separations are the optimum diatomic separations,  $R_{e1}$  for  $M^+...RG$  and  $R_e(RG_2)$  for  $RG...RG$ ; these values are given in Table 1 for  $M = K-Fr$  and in reference 21 for  $M = Li$  and  $Na$ . The corresponding bond angles,  $\theta_{pair}$ , can be straightforwardly calculated and are given in Table 6. We emphasise that this pairwise model, of necessity, predicts the geometries to be bent for all of the Group 1  $M^+RG_2$  complexes, including those for which we have already established a linear geometry.<sup>21</sup> As a consequence it is no surprise that the use of pairwise potentials, such as in refs. 14 and 17, produce such a bent geometry and in fact it is linear geometries which are in need of rationalization. In passing we also note the close agreement of  $\theta_{pair}$  to the fully-optimized bond angle values,  $\theta$ , given in Table 1, for  $M = K-Fr$ .

For  $M =$  Group 2 metal, we have already discussed hybridization of the metal center as a mechanism for obtaining significantly-bound bent structures;<sup>21,42</sup> however, we have also noted that for the Group 1 complexes, such hybridization is not possible since the excitation energy to the lowest unoccupied p and d orbitals is too high (Table 4),<sup>21</sup> confirmed by the contour plots discussed above. In the absence of any other interaction, we would expect weakly-bound bent structures for all  $M^+RG_2$  complexes, including for  $M = Li$  and  $Na$ . Clearly a repulsive interaction is required to overcome the  $RG_2$  interaction energy when moving from bent to linear geometries, and there are two clear sources: Coulomb repulsion and induced-dipole repulsion. The former would arise if there were any charge transfer between the metal center and the RG atoms (and we have noted above that this is small, if it happens at all), while the latter occurs via a polarization of the RG electron density as it interacts with the charge on the metal center. We shall now outline a simple electrostatic model that considers the latter.

### *(ii) Simple Three-Body Model at the Pairwise Geometries*

Assuming no charge transfer, and hence no Coulomb repulsion, in line with the AIM and NPA charges, we give a simple rationalization for the observed geometries in terms of interactions between the induced dipoles on the RG atoms. We commence by considering the complex at the “pairwise geometries”, as discussed above, i.e. a  $C_{2v}$   $M^+RG_2$  complex with each  $M^+...RG$  separation fixed to the optimized value in the  $M^+RG$  diatom,  $R_{e1}$ , the  $RG-RG$

separation fixed to the optimized value in the  $\text{RG}_2$  dimer,  $R_e(\text{RG}_2)$ , and hence with the RG-M-RG bond angle,  $\theta_{\text{pair}}$ , given in Table 6.

A number of workers have considered three-body interactions in depth, which are not straightforward to implement and so still the subject of some controversy.<sup>1,2,3,48</sup> Part of the problem is the reliable inclusion of other terms – dispersion (Axilrod-Teller), exchange and (charge)-induction. One example that has been the subject of some discussion is the exchange quadrupole moment formed on the  $\text{RG}_2$  dimer in the complex, where estimates of parameters in the functional form need to be employed.<sup>2,3</sup> As a consequence, the importance of such terms is unclear, and it has been suggested these may have been overestimated in previous work.<sup>48</sup> Yourshaw et al.<sup>3</sup> have given a very lucid discussion of the different types of interaction term present in both neutral and charged triatoms. In the case of a charged system, it was shown that the non-additive induction term was the largest type of term, with the sum of the exchange charge and multipole dispersion terms approximately balancing the triple-dipole dispersion term, by virtue of these having similar magnitudes and different signs. Since the non-additive induction term is the simplest to calculate with no “fitted” parameters, and is also the largest, we examine the effect of the former on the calculated geometries and binding energies. We find that the inclusion of this single term is sufficient to give close to quantitative agreement for geometries and the binding energy of the second RG atom; later, we shall comment on the other omitted terms.

The positive charge on the metal center will lead to an induced dipole being produced on each RG atom, pointing along the respective  $\text{M}^+$ -RG direction, and these dipoles repel each other. Ignoring higher contributions, the magnitude of the induced dipole,  $\mu_{\text{ind}}$ , on each RG center is given by the standard expression in atomic units:

$$\mu_{\text{ind}} = \frac{\alpha q_{\text{M}}}{R_{\text{e1}}^2} \quad (1)$$

where  $q_{\text{M}}$  is the charge on the metal center,  $\alpha$  is the static dipole polarizability of the RG atom, and  $R_{\text{e1}}$  is the optimized internuclear separation of the  $\text{M}^+$ -RG diatom. The magnitude of the induced dipole will be the same for each RG atom, and in each case be directed along the respective M-RG direction, and oriented from negative to positive (i.e. pointing towards the metal center) – see Figure 3. Stone<sup>49,50</sup> has considered the interaction between two such dipoles in a general way, and we use a version of his equation for the interaction between the two dipoles in the present system. As may be seen from Figure 3, the induced dipoles are in the same plane and make angles  $\theta_{\text{A}}$  and  $\theta_{\text{B}}$  to a line passing through both of the RG centers. The expression for the interaction energy between these two induced dipoles,  $U_{\mu\mu}$ , in atomic units is given by:

$$U_{\mu\mu} = -\frac{\mu_{\text{ind}}^2}{R_{\text{RG-RG}}^3} (2\cos\theta_{\text{A}}\cos\theta_{\text{B}} - \sin\theta_{\text{A}}\sin\theta_{\text{B}}) \quad (2)$$

where, in the present model (at the pairwise geometry),  $R_{\text{RG-RG}}$  takes the value  $R_e(\text{RG}_2)$  in Eq. 2. We have calculated this induced dipole repulsion for all  $\text{M}^+-\text{RG}_2$  complexes ( $\text{M} = \text{Li-Fr}$  and  $\text{RG} = \text{He-Rn}$ ), and tabulate these in Table 6. The  $U_{\mu\mu}$  values have been calculated with an assumed metal charge of +1.00 (and hence the charge on the RG atom is zero). Also in this table we give the calculated dissociation energies of the  $\text{RG}_2$  complexes using the quintuple- $\zeta$  basis sets described earlier for  $\text{M} = \text{K-Fr}$  and the triple- $\zeta$  ones noted in reference 21 and used for  $\text{M} = \text{Li}$  and  $\text{Na}$ .

We see from Table 6 that for the cases of  $\text{M} = \text{Li}$  and  $\text{Na}$ , the repulsive induced-dipole interaction is greater than  $D_e(\text{RG}_2)$  in all cases except for  $\text{Na}^+-\text{Ne}_2$ , and thus the  $\text{RG}\dots\text{RG}$  interaction is overcome and these complexes prefer a linear geometry; on the other hand, for the complexes with  $\text{M} = \text{K-Fr}$ ,  $U_{\mu\mu}$  is less than  $D_e(\text{RG}_2)$  and it can be seen that in these cases the complex retains a bent geometry. (In the case of  $\text{Na}^+-\text{Ne}_2$ ,  $U_{\mu\mu}$  and  $D_e(\text{RG}_2)$  are very close and this would be consistent with a floppy, quasilinear complex.) Although this model is very simple – it gives a clear rationale for the observed geometries. As will be seen shortly, it is actually a close to quantitative model for the Group 1  $\text{M}^+-\text{RG}_2$  complexes.

### (iii) 3-Body Model at the Optimized Geometry

We now consider the interactions which are present at our quantum chemical equilibrium geometry for each  $\text{M}^+-\text{RG}_2$  complex. The emphasis here is on the examination of the three-body term contribution to the angular potential and so we use a quantum chemical representation of the  $\text{RG-RG}$  potential. Hence, to test this simple model more quantitatively, we have calculated the  $\text{RG}_2$  potential as a function of the  $\text{RG}\dots\text{RG}$  internuclear separation,  $U_{\text{RG-RG}}$ , using the corresponding method and basis sets. At each  $\text{RG}\dots\text{RG}$  separation in the  $\text{M}^+-\text{RG}_2$  complex, we have calculated the induced-dipole repulsion term,  $U_{\mu\mu}$ , using Eq. 2, assuming the  $\text{M}^+\dots\text{RG}$  internuclear separation remains fixed at the value in the optimized complex. We can identify the interaction term for the addition of the second RG atom,  $U_{\text{MRG-RG}}$ , as:

$$U_{\text{MRG-RG}} = U_{\mu\mu} + U_{\text{RG-RG}} + D_{e1} \quad (3)$$

This is calculated at each  $\text{RG}\dots\text{RG}$  separation, and we plot the results in Figure 4 for selected  $\text{M}^+-\text{RG}_2$  ( $\text{M} = \text{Li, Na}$ ) complexes, and in Figure 5 for selected heavier  $\text{M}^+-\text{RG}_2$  ( $\text{M} = \text{K-Fr}$ ) complexes.

We first consider the cases of  $\text{M} = \text{Li}$  and  $\text{Na}$ . It may be seen from the electrostatic potentials in Figure 4 that the angular potentials are very flat, in agreement with the conclusions of ref. 21 (see Fig. 3 of that work). Additionally, all of the  $\text{M} = \text{Li}$  complexes show linear global minima, with no bent local minima. We note that a few of the complexes did in fact show very shallow bent minima for  $\text{M} = \text{Li}$  in the quantum calculations of ref. 21, but these were extremely shallow. (We also note that in the present model we have not allowed the  $\text{M}^+-\text{RG}$  bond length to relax.) For  $\text{M} = \text{Na}$ , we note that the potentials in Fig. 4 show bent global

minima, with a very broad plateau around linearity. The quantum chemical calculations of ref. 21 actually showed global linear minima, but did show bent local minima. Again, with the approximations in the present approach and the shallowness of the potentials, these effects, although small, can have an effect on the resultant minimum energy angle. Overall, though, the similarity of the quantum chemical curves and the present electrostatic ones is striking. We also note that in ref. 16 the  $\text{Na}^+\text{-Ar}_2$  complex was concluded to be linear, and that this was attributable to the three-body terms, although both induced-dipole and Axilrod-Teller terms were considered simultaneously.

Moving onto the heavier metals,  $M = \text{K-Fr}$ , we see that the electrostatic potentials in Fig. 5 look very similar to the quantum chemical ones in Fig. 2, with a bent global minimum. This bent minimum is driven by two factors: the more deeply-bound RG-RG interaction potential,  $U_{\text{RG-RG}}$ , with increasing atomic number of RG, and the smaller induced dipole on the RG atoms caused by the corresponding increasing  $R_{e2}$  values, and hence smaller repulsion term between these, exacerbated by the larger size of the RG atoms.

For all complexes, we identify the minimum value of  $U_{\text{MRG-RG}}$  from Eq. 3 and the results are given in Table 7, where we compare these values to the respective  $D_{e2}$  values. As may be seen, the agreement between the calculated minimum in this simple model and  $D_{e2}$  is almost quantitative. Coupled with our previous work on the diatomic  $M^+\text{-RG}$  complexes,<sup>40</sup> and known behaviour of  $\text{RG}_2$ , the current results strongly confirm the expectation that the interactions in the Group 1  $M^+\text{-RG}_2$  complexes are almost wholly physical, and that the three-body interaction is well-described by a single electrostatic term. We also include the value of  $R$  at which this minimum value of  $U_{\text{MRG-RG}}$  occurs, denoted  $R_{\text{ind}}(\text{RG}_2)$ , which can also be seen to be in good agreement with the quantum chemical minimum (noting the latter occurs from a full optimization, while the former is estimated from a rather coarse pointwise potential).

We noted above that the  $D_{e2}/D_{e1}$  ratios are quite close to unity (see Table 1), but are always greater; additionally, the ratios generally increase with both the atomic number of  $M$  and RG. Our analysis of the electrostatic model shows that this arises as the induced dipoles become smaller with increasing atomic number of  $M$  and RG owing to the increased  $M^+\dots\text{RG}$  separation (Table 1 and Figure 1), and for the RG atoms, this overrides the increasing polarizability, although the latter has an effect in that it is increasing  $U_{\text{RG-RG}}$ .

Finally, in Figure 6 we show a comparison of angular plots using three approaches for three selected  $M^+\text{-RG}_2$  complexes to represent the range of the series:  $\text{Li}^+\text{-He}_2$ ,  $\text{K}^+\text{-Ar}_2$  and  $\text{Cs}^+\text{-Xe}_2$ . It is immediately clear that the pairwise potentials give bent geometries for all three complexes (and indeed will always do so); additionally, the pairwise well depths are significantly overestimated compared to the electrostatic and quantum chemical potentials, showing the significance of the induced dipole repulsion term. For the latter two, there is very good agreement through a wide range of the angles, in particular covering the bent minima of  $\text{K}^+\text{-Ar}_2$  and  $\text{Cs}^+\text{-Xe}_2$ . In all cases, there is a gradual deviation between the electrostatic and quantum chemical curves towards linearity. A small part of this is the non-optimal values of the  $M^+\dots\text{RG}$  internuclear separation; however, this is small amounting to only a few  $\text{cm}^{-1}$

even in the case of  $\text{Cs}^+\text{-Xe}_2$ . That the agreement is so good over a wide range of angles, suggests that other terms (exchange, dispersion etc.) are either small or they fortuitously cancel, and we shall comment further on this below. Even though there is a large disparity between the well depths of the pairwise potential, and those of the electrostatic and quantum chemical approaches (which are very similar to each other), all potentials give very similar equilibrium bond angles for  $M = \text{K-Fr}$ .

#### 4. FURTHER COMMENTS AND CONCLUSIONS

Bauschlicher et al.<sup>20</sup> appear to be the first authors to have discussed the hybridization of Group 2 metal cations when interacting with two RG atoms, with a view to providing an explanation for the observed bent geometry of  $\text{Mg}^+\text{-Ar}_2$ ; an explanation we expanded in our work rationalizing the bent and linear geometries of the Group 2  $M^+\text{-RG}_2$  complexes.<sup>21,42</sup> What was omitted from refs. 20 and 21 was the realization that there was actually a need for an explanation as to why the  $\text{Li}^+\text{-RG}_2$  and  $\text{Na}^+\text{-RG}_2$  complexes were linear (or quasilinear). Indeed, we have noted above that in the pairwise approximation it would be expected that all  $M^+\text{-RG}_2$  complexes would be bent, with the atoms at their optimum  $M^+\text{-RG}$  and  $\text{RG-RG}$  separations. We have now shown that the  $M^+\text{-RG}_2$  complexes with  $M = \text{K - Fr}$  are all bent, which is in line with expectations from a pairwise picture although the predicted binding energies are significantly different for the latter model. We have shown that the introduction of the induced dipole repulsion term explains both the observed bent geometries and the (quasi)linear ones for the  $M = \text{Li}$  and  $\text{Na}$  complexes. Indeed, this repulsion term appears to be the key to understanding the linear structures: if this is greater than the  $\text{RG}_2$  binding energy, then linear equilibrium geometries result; if not, then bent geometries result. Although perhaps obvious, particularly in retrospect, this appears to be the first time that such geometries have been examined in detail consistently for an elemental group, and a clear explanation of the trend given.

It is remarkable that such a simple model gives such agreement with the results of good-quality quantum chemical calculations, both qualitatively and quantitatively (see Figure 6); by extension, we would expect this to be the case for other complexes that are physically bound. We have noted that there are other three-body terms that could be included,<sup>1,2,3</sup> but the results in the present work suggest that either: (i) such terms are small with respect to the induced dipole repulsion interaction; or (ii) there is fortuitous cancellation of such terms, at least close to the bent equilibrium geometries. The latter is more in line with the results reported for halide/argon complex anions;<sup>3</sup> however, the difference in sign of the charged species is clearly a major difference here, which would lead to some of the cancellation becoming enhancements. We suggest that the lower polarizability of a cation over an anion is enough to lead to a significant diminution of the omitted terms. In addition, the shorter equilibrium separations in cationic species will lead to an enhancement of the induced dipole repulsion term. It would be of interest to pursue this in further studies, to see if such terms could explain the observed discrepancies observed close to linearity and what the effect of higher-level quantum chemical calculations would be; however, the present very good

agreement for thirty six complexes from  $\text{Li}^+\text{-He}$  to  $\text{Fr}^+\text{-Rn}$  suggests the single three-body term is largely sufficient for the present set of cationic complexes.

We emphasise that in cases where hybridization occurs, such as for the Group 2 complexes,<sup>21,42</sup> the energy gain from hybridization is likely to outweigh the induced-dipole effect; indeed, NPA and AIM analyses suggest that in some cases charge transfer may also be present in those species and hence the situation will be more complicated than for the current Group 1, or other physically-bound complexes – we shall consider this further in future work – such comments likely apply to more “usual” ligands such as water.

The apparent success of the addition of a single term to three-body potentials suggests that it would be useful to investigate this simple addition to pairwise potentials of physically-bound species in wider-ranging studies to see the effect on larger complexes.

## **ACKNOWLEDGMENTS**

The authors are thankful to the NSCCS and University of Nottingham HPC facility for the provision of computing time. A.A. is grateful to the EPSRC and The University of Nottingham for the provision of a studentship. W.H.B is grateful to the Department of Chemistry at the University of Utah for travel funding, allowing visits to the University of Nottingham. Dr. R. J Wheatley (Nottingham) is thanked for extremely useful discussions.

**Table 1:** Spectroscopic Parameters for  $M^+ - RG_2$  ( $M= K-Fr$  and  $RG = He$  to  $Rn$ )<sup>a</sup>

RG	$R_{e2}/\text{\AA}$	$R_{e1}/\text{\AA}$	$R_{e2}/R_{e1}$	$\theta/^\circ$	$R_{RG-RG}/\text{\AA}$	$R_e(RG_2)$	$R_{RG-RG}/R_e(RG_2)$	$D_{e2}/\text{cm}^{-1}$	$D_{e1}/\text{cm}^{-1}$	$D_{e2}/D_{e1}$
<b>K<sup>+</sup></b>										
He	2.822	2.825	1.00	67.0	3.115	3.079	1.01	190	187	1.02
Ne	2.922	2.921	1.00	68.0	3.268	3.194	1.02	348	336	1.04
Ar	3.200	3.214	1.00	74.5	3.874	3.760	1.03	954	913	1.04
Kr	3.334	3.325	1.00	76.7	4.137	3.980	1.04	1198	1156	1.04
Xe	3.532	3.513	1.00	79.4	4.512	4.338	1.04	1527	1491	1.02
Rn	3.609	3.595	1.00	80.2	4.650	4.444	1.05	1722	1690	1.02
<b>Rb<sup>+</sup></b>										
He	3.050	3.070	0.99	60.9	3.090	3.079	1.00	159	154	1.03
Ne	3.134	3.140	1.00	62.4	3.248	3.194	1.02	299	283	1.06
Ar	3.396	3.423	0.99	69.0	3.846	3.760	1.02	850	788	1.08
Kr	3.528	3.521	1.00	71.1	4.105	3.980	1.03	1073	1002	1.07
Xe	3.722	3.712	1.00	74.1	4.483	4.338	1.03	1370	1288	1.06
Rn	3.806	3.792	1.00	74.5	4.607	4.444	1.04	1549	1460	1.06
<b>Cs<sup>+</sup></b>										
He	3.297	3.359	0.98	56.3	3.111	3.079	1.01	147	139	1.06
Ne	3.350	3.398	0.99	58.2	3.258	3.194	1.02	280	262	1.07
Ar	3.574	3.571	1.00	64.7	3.825	3.760	1.02	823	754	1.09
Kr	3.697	3.693	1.00	66.9	4.076	3.980	1.02	1051	966	1.09
Xe	3.888	3.882	1.00	69.8	4.449	4.338	1.03	1343	1234	1.09
Rn	3.966	3.958	1.00	70.4	4.572	4.444	1.03	1521	1395	1.09
<b>Fr<sup>+</sup></b>										
He	3.401	3.404	1.00	54.1	3.093	3.079	1.00	130	124	1.05
Ne	3.443	3.440	1.00	56.1	3.238	3.194	1.01	259	242	1.07
Ar	3.646	3.644	1.00	63.1	3.815	3.760	1.01	801	726	1.10
Kr	3.763	3.760	1.00	65.5	4.071	3.980	1.02	1034	938	1.10
Xe	3.949	3.944	1.00	68.5	4.445	4.338	1.02	1331	1206	1.10
Rn	4.024	4.017	1.00	69.1	4.564	4.444	1.03	1516	1371	1.11

<sup>a</sup>  $R_{e2}$  is the  $M^+ - RG$  equilibrium bond length in  $M^+ - RG_2$ , where  $R_{e1}$  is the  $M^+ - RG$  equilibrium bond length in  $M^+ - RG$ .  $\theta$  is the  $RG - M^+ - RG$  bond angle,  $D_{e2}$  is the dissociation energy of  $M^+ - RG + RG$  and  $D_{e1}$  is the dissociation energy of  $M^+ - RG$ .  $R_{RG-RG}$  is the  $RG - RG$  internuclear distance in the  $M^+ - RG_2$  complex;  $R_e(RG_2)$  is the optimized  $RG_2$   $R_e$  value. For the geometries and interaction energies values were obtained at the RMP2/aV5Z level of theory (see text.)

**Table 2:** Harmonic vibrational frequencies for  $M^+ \text{-RG}_2$  ( $M = \text{K, Rb, Cs}$  and  $\text{Fr}$ ;  $\text{RG}_2 = \text{He}$  to  $\text{Rn}$ ) species obtained at the RMP2/aV5Z level of theory (see text).<sup>a</sup>

Rare Gas	$\nu_1/\text{cm}^{-1}$	$\nu_2/\text{cm}^{-1}$	$\nu_3/\text{cm}^{-1}$
<b>K<sup>+</sup></b>			
He	109	22	104
Ne	77	20	67
Ar	90	26	77
Kr	81	18	68
Xe	77	14	66
Rn	76	12	65
<b>Rb<sup>+</sup></b>			
He	91	24	89
Ne	61	19	55
Ar	70	26	61
Kr	60	19	50
Xe	56	17	47
Rn	52	14	43
<b>Cs<sup>+</sup></b>			
He	80	23	79
Ne	53	18	49
Ar	62	23	55
Kr	52	20	44
Xe	48	17	40
Rn	44	15	36
<b>Fr<sup>+</sup></b>			
He	76	24	75
Ne	50	20	47
Ar	58	25	52
Kr	47	20	41
Xe	41	13	35
Rn	38	14	31

<sup>a</sup>  $\nu_1$  and  $\nu_2$  correspond to the symmetric stretching and bending motions,  $\nu_3$  is the asymmetric stretch.

**Table 3:** Calculated charges on the metal center,  $q_M$ , in the titular  $M^+-RG_2$  and  $M^+-RG$  species.<sup>a</sup>

	$M^+-RG_2$				$M^+-RG$			
	$K^+$	$Rb^+$	$Cs^+$	$Fr^+$	$K^+$	$Rb^+$	$Cs^+$	$Fr^+$
He	<b>1.00</b> [1.00] (1.00)	<b>1.00</b> [1.00] (1.01)	<b>1.00</b> [1.00] (1.01)	<b>1.00</b> [1.00] (1.01)	<b>1.00</b> [1.00] (1.00)	<b>1.00</b> [1.00] (1.00)	<b>1.00</b> [1.00] (1.00)	<b>1.00</b> [1.00] (1.01)
Ne	<b>0.99</b> [1.00] (0.99)	<b>1.00</b> [1.00] (0.99)	<b>1.00</b> [1.00] (0.99)	<b>1.00</b> [1.00] (0.99)	<b>1.00</b> [1.00] (1.00)	<b>1.00</b> [1.00] (1.00)	<b>1.00</b> [1.00] (1.00)	<b>1.00</b> [1.00] (1.00)
Ar	<b>0.98</b> [0.99] (0.99)	<b>0.98</b> [0.99] (0.99)	<b>0.99</b> [0.99] (0.99)	<b>0.98</b> [0.99] (1.01)	<b>0.99</b> [1.00] (0.99)	<b>0.99</b> [1.00] (1.00)	<b>0.99</b> [1.00] (0.99)	<b>0.99</b> [1.00] (1.01)
Kr	<b>0.97</b> [0.98] (0.94)	<b>0.98</b> [0.98] (0.94)	<b>0.98</b> [0.99] (0.95)	<b>0.98</b> [0.99] (0.94)	<b>0.98</b> [0.99] (0.97)	<b>0.99</b> [1.00] (0.97)	<b>0.99</b> [1.00] (0.97)	<b>0.99</b> [1.00] (0.97)
Xe	<b>0.96</b> [0.97] (0.90)	<b>0.96</b> [0.98] (0.90)	<b>0.96</b> [0.98] (0.93)	<b>0.96</b> [0.98] (0.92)	<b>0.98</b> [0.99] (0.95)	<b>0.98</b> [0.99] (0.95)	<b>0.98</b> [0.99] (0.96)	<b>0.98</b> [0.99] (0.96)
Rn	<b>0.95</b> [0.97] (0.91)	<b>0.96</b> [0.97] (0.89)	<b>0.96</b> [0.98] (0.93)	<b>0.96</b> [0.98] (0.92)	<b>0.97</b> [0.99] (0.95)	<b>0.97</b> [0.99] (0.94)	<b>0.98</b> [0.99] (0.96)	<b>0.98</b> [0.99] (0.96)

<sup>a</sup> AIM results presented in bold, NPA results are in square brackets, and Mulliken results are in parentheses. The charge on the RG atom can be found from  $0.5 \times (1 - q_M)$

**Table 4:** Atomic Properties

Species	Lowest Transition <sup>43</sup>	Lowest Transition Energy/ cm <sup>-1</sup> 43	Static dipole Polarizability / Å <sup>3</sup> 39	Ionization Energy / cm <sup>-1</sup> 43
K <sup>+</sup>	$^1P_1 (3p^5 4s) \leftarrow ^1S_0 (3p^6)$	166 457		
Rb <sup>+</sup>	$^2[3/2]_1^0 (4p^5(^2P_{3/2}^0)5s) \leftarrow ^1S_0 (4p^6)$	134 870		
Cs <sup>+</sup>	$^2[3/2]_1^0 (5p^5(^2P_{3/2}^0)6s) \leftarrow ^1S_0 (5p^6)$	110 954		
Fr <sup>+</sup>	Not available	Not available	Not available	Not available
He			0.205	198 311
Ne			0.396	173 930
Ar			1.642	127 110
Kr			2.519	112 914
Xe			4.044	97 834
Rn			5.103	86 693

**Table 5:** Energy differences ( $\text{cm}^{-1}$ ) between the linear and (lower energy) bent minima for  $\text{M}^+\text{-RG}_2$  ( $\text{M} = \text{K-Fr}$ ;  $\text{RG} = \text{He- Rn}$ ) calculated at the MP2/aV5Z level (see text)

<b>Rare Gas</b>	<b>Metal Cation</b>			
	$\text{K}^+$	$\text{Rb}^+$	$\text{Cs}^+$	$\text{Fr}^+$
He	2	3	8	8
Ne	10	15	18	20
Ar	63	77	97	99
Kr	85	110	125	145
Xe	113	146	177	198
Rn	137	172	209	239

**Table 6:** Calculated induced-dipole/induced-dipole interaction energies ( $\text{cm}^{-1}$ ) for the  $\text{M}^+\text{-RG}_2$  complexes and dissociation energies for the  $\text{RG}_2$  dimers. The  $\text{M}^+\text{-RG}$  internuclear separations have been fixed at the  $R_{e1}$  value (see Table 1), and the  $\text{RG-RG}$  separation has been fixed at  $R_e(\text{RG}_2)$  (see Table 1), these parameters then fix the  $\text{RG-M-RG}$  bond angle,  $\theta$ .

M	$\theta_{\text{pair}} / ^\circ$	$U_{\text{ind}} / \text{cm}^{-1}$	$D_e(\text{RG}_2)$
RG = He			
Li	108.6	21	5 <sup>a</sup>
Na	82.6	8	
K	66.0	3	5 <sup>b</sup>
Rb	60.2	2	
Cs	54.6	2	
Fr	53.8	2	
RG = Ne			
Li	101.1	52	29 <sup>a</sup>
Na	79.0	21	
K	66.3	10	22 <sup>b</sup>
Rb	61.1	7	
Cs	56.1	5	
Fr	55.3	5	
RG = Ar			
Li	104.4	297	111 <sup>a</sup>
Na	84.3	138	
K	71.6	74	113 <sup>b</sup>
Rb	66.6	56	
Cs	63.5	46	
Fr	62.1	42	
M = Kr			
Li	105.9	458	157 <sup>a</sup>
Na	86.3	221	
K	73.5	126	163 <sup>b</sup>
Rb	68.8	97	
Cs	65.2	79	
Fr	63.9	73	
M = Xe			
Li	106.2	731	250 <sup>a</sup>
Na	88.2	379	
K	76.3	211	237 <sup>b</sup>
Rb	71.5	164	
Cs	67.9	134	
Fr	66.7	125	
M = Rn			
Li	104.9	973	313 <sup>a</sup>
Na	87.6	514	
K	76.4	285	297 <sup>b</sup>
Rb	71.7	224	
Cs	70.6	185	
Fr	67.2	173	

<sup>a</sup> Using aug-cc-pVTZ triple-zeta quality basis sets, as used in ref. 21.

<sup>b</sup> Using quintuple-zeta basis sets, as employed in the present work.

**Table 7:** Electrostatic model quantities compared to those from quantum chemical calculations.

M	$-U_{\text{MRG-RG}}/\text{cm}^{-1}$	$D_{e2}/\text{cm}^{-1}$	$R_{\text{ind}}(\text{RG}_2)/\text{\AA}$	$R_{\text{RG-RG}}/\text{\AA}$
He				
K	189	190	3.15	3.115
Rb	157	159	3.15	3.090
Cs	142	147	3.10	3.111
Fr	127	130	3.10	3.093
Ne				
K	348	348	3.25	3.268
Rb	297	299	3.25	3.248
Cs	278	280	3.20	3.258
Fr	259	259	3.20	3.238
Ar				
K	952	954	3.8	3.874
Rb	840	850	3.8	3.846
Cs	821	823	3.8	3.825
Fr	797	801	3.8	3.815
Kr				
K	1199	1198	4.1	4.137
Rb	1071	1073	4.1	4.105
Cs	1052	1051	4.1	4.076
Fr	1030	1034	4.0	4.071
Xe				
K	1530	1527	4.5	4.512
Rb	1367	1370	4.5	4.483
Cs	1341	1343	4.4	4.449
Fr	1322	1331	4.4	4.445
Rn				
K	1718	1722	4.6	4.650
Rb	1544	1549	4.6	4.607
Cs	1513	1521	4.6	4.572
Fr	1500	1516	4.5	4.564

**Figure 1:** HF HOMO contour plots for  $M^+ - RG_2$  complexes ( $M = K, Rb, Cs$  and  $Fr$ ;  $RG =$  rare gas). The contour spacings employed are the same for all species.

**Figure 2:** Selected minimum energy angular paths for selected Group 1  $M^+ - RG_2$  angular plots where a)  $RG = He$  b)  $RG = Ar$  and c)  $RG = Xe$ . The zero on the interaction energy axis corresponds to the  $M^+ - RG + RG$  asymptote.

**Figure 3:** Diagram showing the parameters involved in the electrostatic model underlying the bent/linear geometries – see text.

**Figure 4:** Angular plots of  $U_{MRG-RG}$  for  $M^+ - RG_2$ ,  $M = Li, Na$  – see text for details. The zero on the interaction energy axis corresponds to the  $M^+ - RG + RG$  asymptote.

**Figure 5:** Angular plots of  $U_{MRG-RG}$  for  $M^+ - RG_2$ ,  $M = K-Fr$  – see text for details. The zero on the interaction energy axis corresponds to the  $M^+ - RG + RG$  asymptote.

**Figure 6:** Comparison of quantum chemical angular plots (from Figure 2) with equivalent electrostatic model plots (from Figures 6 and 7). The deviations for small bond angles are due to the fixed internuclear separations in the electrostatic model; the deviations at angles close to linearity are thought to be due to higher-order terms coupled with their angular dependence, together with a greater propensity for (small amounts of) charge transfer. The zero on the interaction energy axis corresponds to the  $M^+ - RG + RG$  asymptote.

Figure 1:

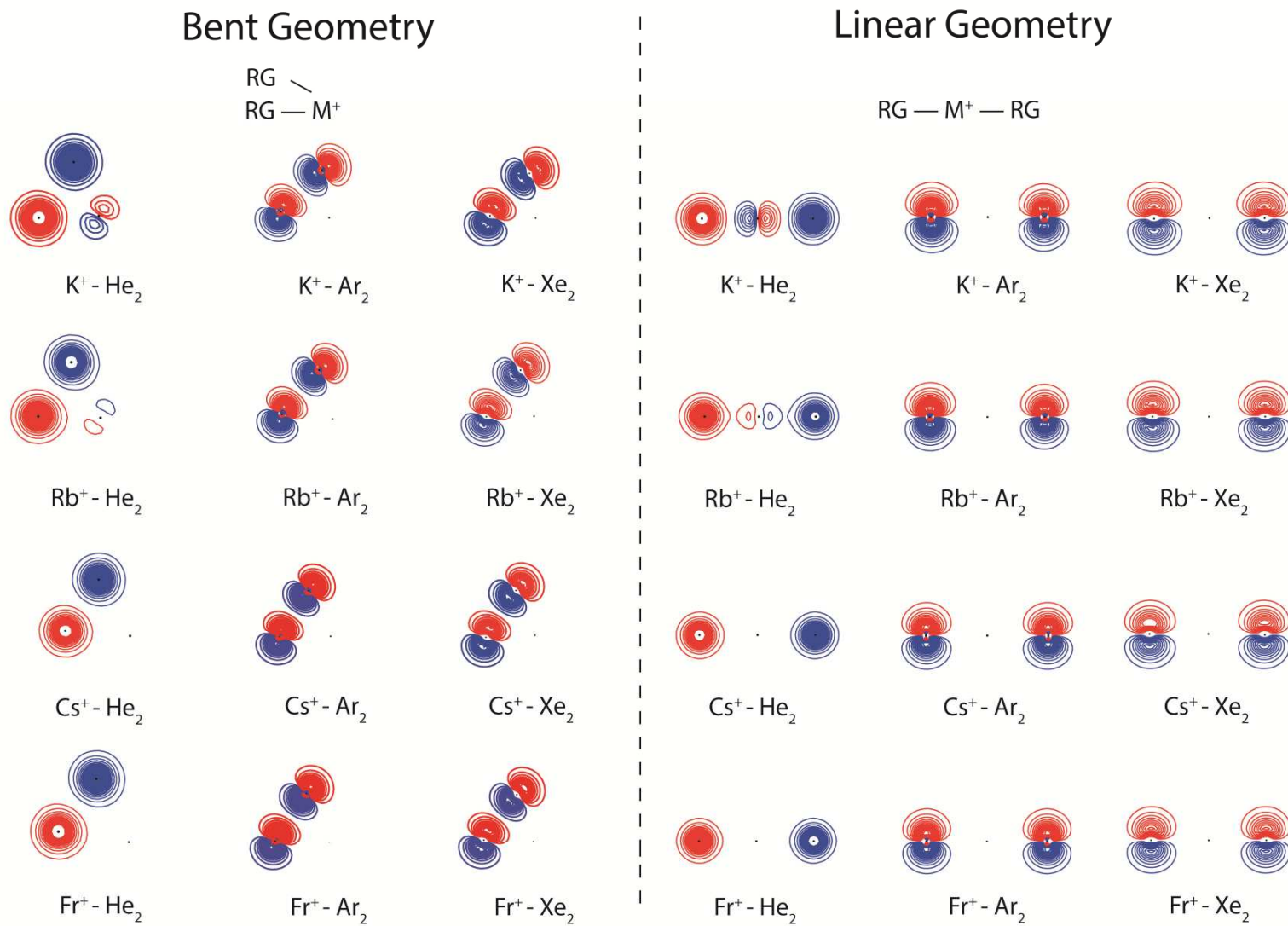
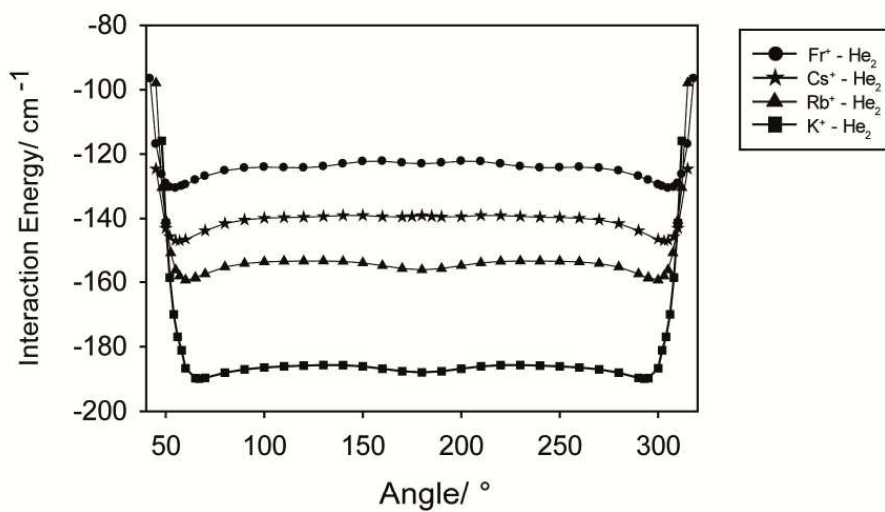
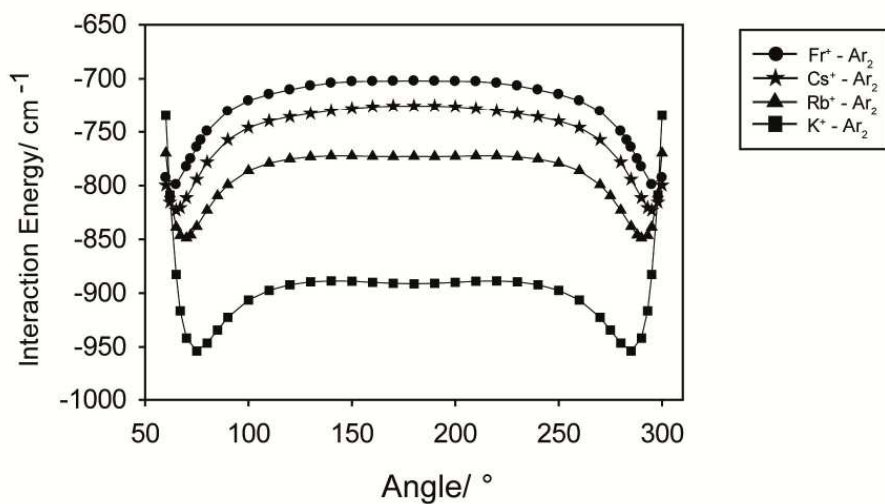


Figure 2:

a)



b)



c)

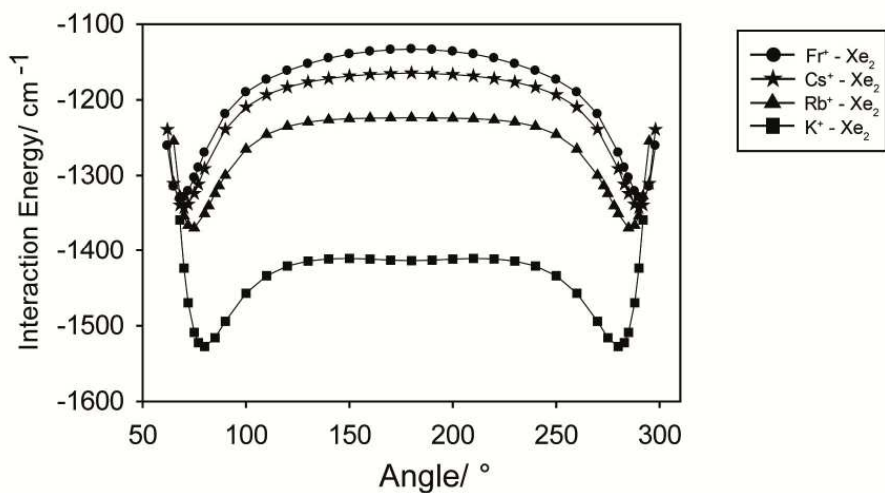


Figure 3:

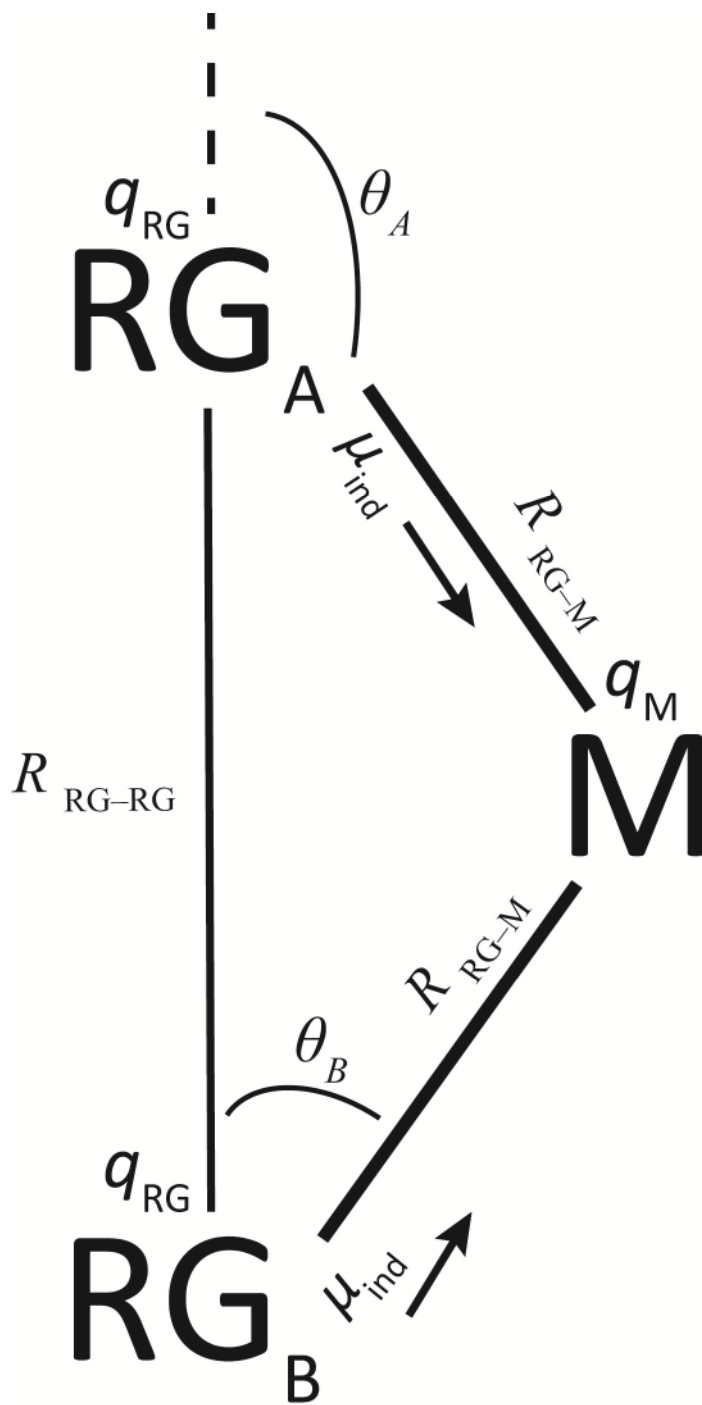


Figure 4

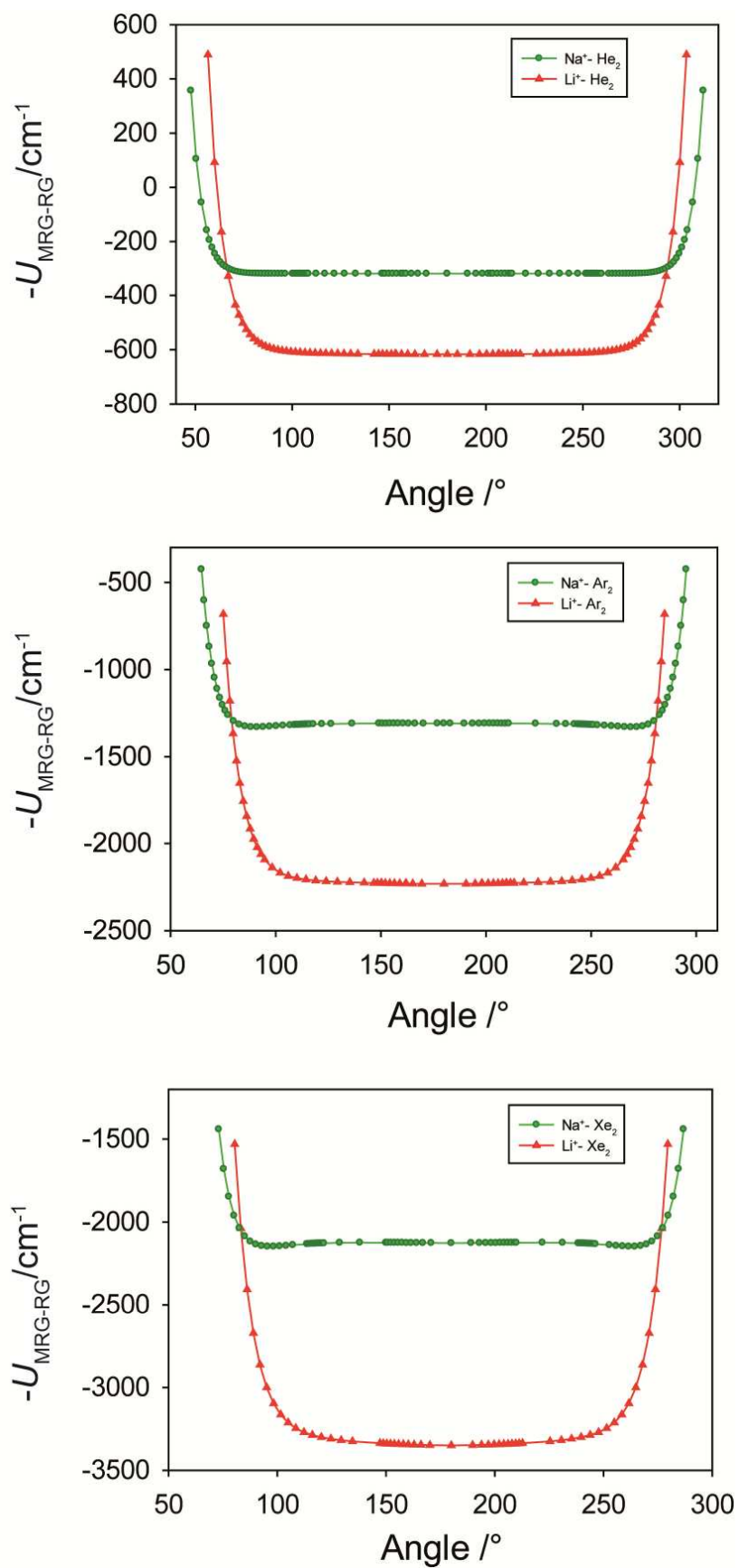


Figure 5

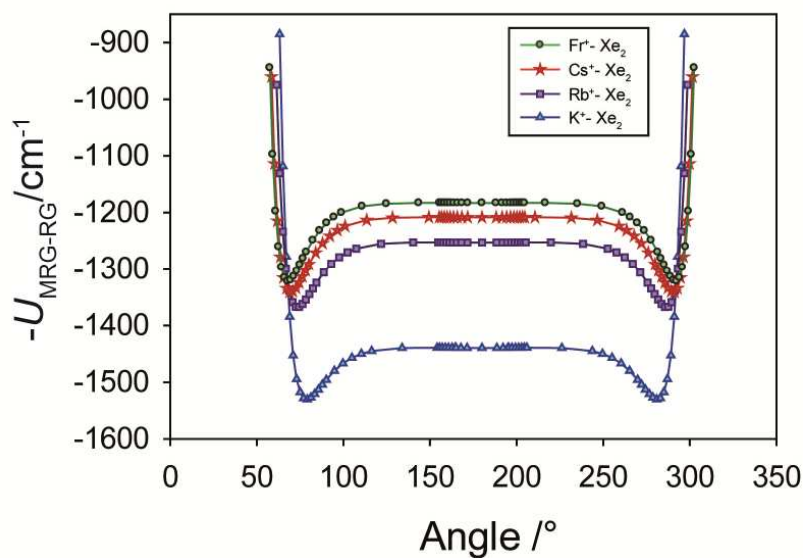
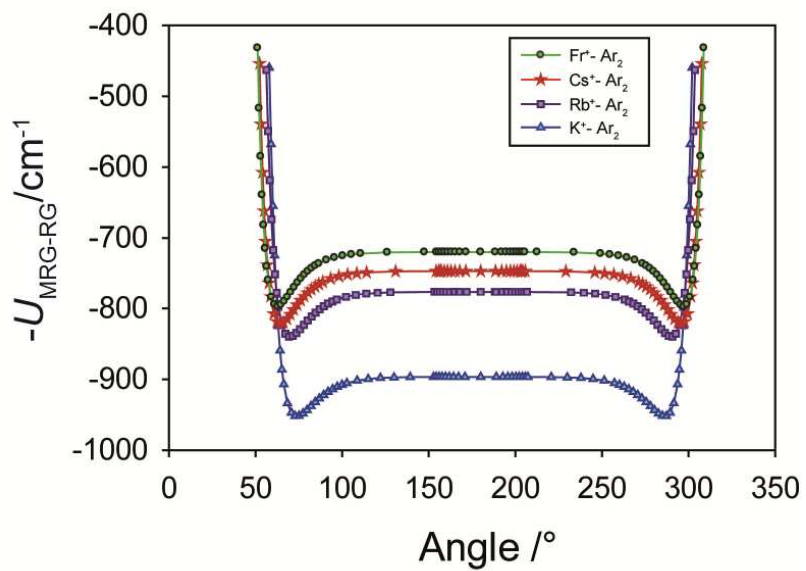
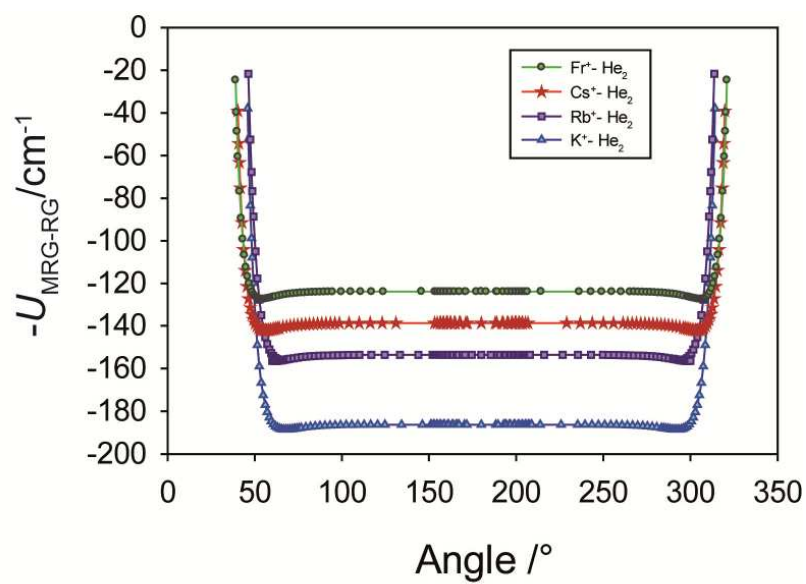
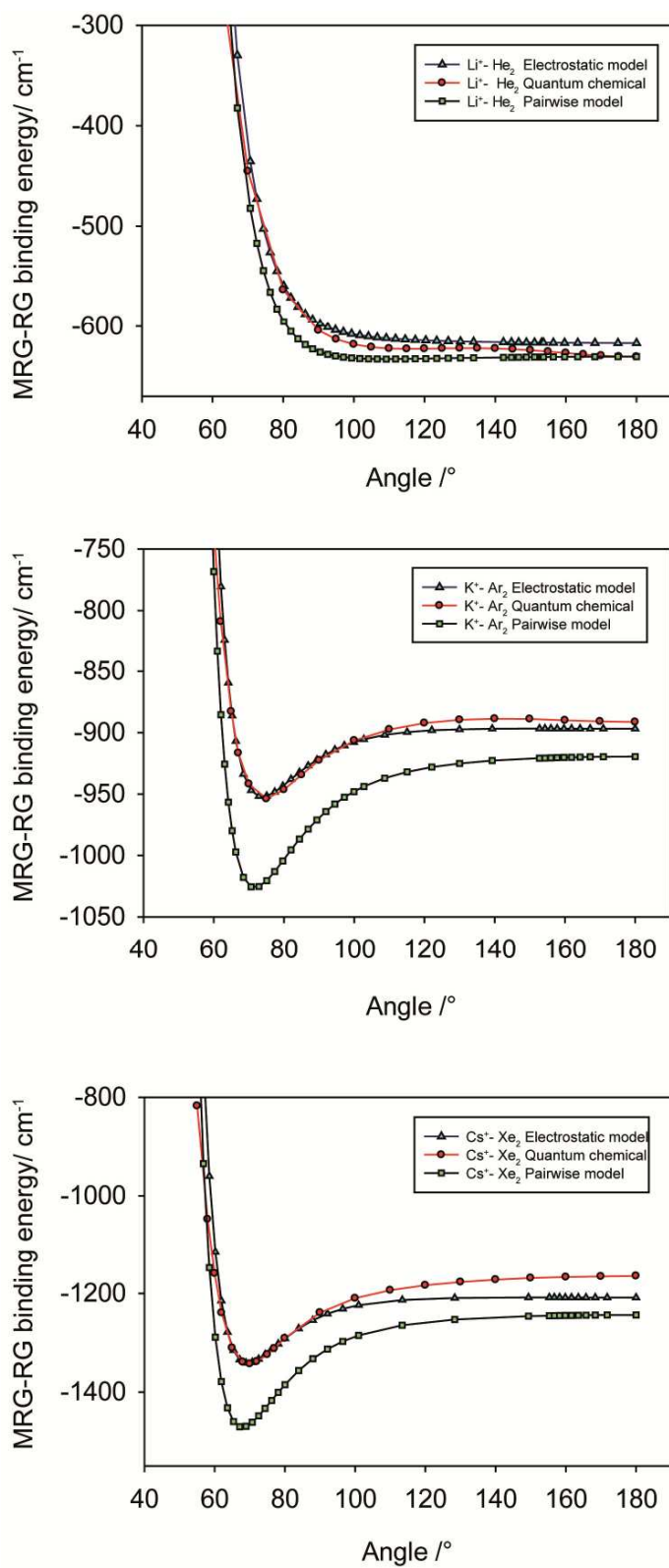
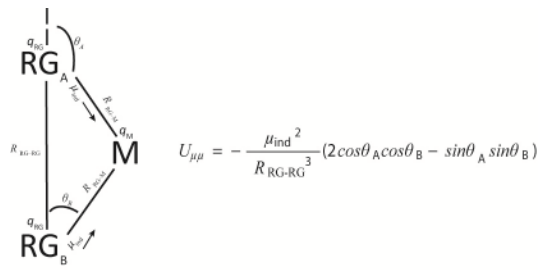


Figure 6



# TOC Image



$$U_{\mu\mu} = - \frac{\mu_{ind}^2}{R_{RG-RG}^3} (2 \cos \theta_A \cos \theta_B - \sin \theta_A \sin \theta_B)$$

## References

- 
- <sup>1</sup> Reilly, A. M.; Tkatchenko, A. van der Waals dispersion interactions in molecular materials: beyond pairwise additivity. *Chem. Sci.* **2015**, *6*, 3289–3301.
- <sup>2</sup> Hutson, J. M.; Liu, S.; Moskowitz, J. W.; Bačić, Z. Nonadditive intermolecular forces in Ar<sub>n</sub>-HF van der Waals clusters: effects on the HF vibrational frequency shift. *J. Chem. Phys.* **1999**, *111*, 8378–8383.
- <sup>3</sup> Yourshaw, I.; Zhao, Y.; Neumark, D. M. Many-body effects in weakly bound anion and neutral clusters: zero electron kinetic energy spectroscopy and threshold photodetachment spectroscopy of Ar<sub>n</sub>Br<sup>-</sup> (n=2-9) and Ar<sub>n</sub>I (n=2-19). *J. Chem. Phys.* **1996**, *105*, 351–373.
- <sup>4</sup> Bellert, D.; Breckenridge, W. H. Bonding in ground-state and excited-state A<sup>+</sup>•Rg van der Waals ions (A= atom, Rg= rare-gas atom): a model-potential analysis. *Chem. Rev.* **2002**, *102*, 1595–1622.
- <sup>5</sup> Hickling, H. L.; Viehland, L. A.; Shepherd, D. T.; Soldan, P.; Lee, E. P. F.; Wright, T. G. Spectroscopy of M<sup>+</sup>.Rg and transport coefficients of M<sup>+</sup> in Rg (M = Rb-Fr; Rg = He-Rn). *Phys. Chem. Chem. Phys.* **2004**, *6*, 4233–4239
- <sup>6</sup> Vieland, L. A.; Lozeille, J.; Soldan, P.; Lee, E. P. F.; Wright, T. G. Spectroscopy of K<sup>+</sup>.Rg and transport coefficients of K<sup>+</sup> in Rg (Rg = He-Rn). *J. Chem. Phys.* **2004**, *121*, 341–351.
- <sup>7</sup> Gardner, A. M.; Withers, C. D.; Wright, T. G.; Kaplan, K. I.; Chapman, C. Y. N.; Viehland, L. A.; Lee, E. P. F.; Breckenridge, W. H. Theoretical study of the bonding in M<sup>n+</sup>-RG complexes and the transport of M<sup>n+</sup> through RG (M = Ca, Sr, Ra; n = 1,2; RG = He-Rn). *J. Chem. Phys.* **2010**, *132*, 054302–11.
- <sup>8</sup> Gardner, A. M.; Withers, C. D.; Graneek, J. B.; Wright, T. G.; Viehland, L. A.; Breckenridge, W. H. Theoretical study of M<sup>+</sup>-RG and M<sup>2+</sup>-RG complexes and transport of M<sup>+</sup> through RG (M = Be and Mg; RG = He-Rn). *J. Phys. Chem. A* **2010**, *114*, 7631–7641
- <sup>9</sup> McGuirk, M. F.; Viehland, L. A.; Lee, E. P. F.; Breckenridge, W. H.; Withers, C. D.; Gardner, A. M.; Plowright, R. J.; Wright, T. G. Theoretical study of Ba<sup>n+</sup>-RG complexes and transport of Ba<sup>n+</sup> through RG (RG = He-Rn). *J. Chem. Phys.* **2009**, *130*, 194305–9
- <sup>10</sup> Harris, J. P.; Gardner, A. M.; Wright, T. G.; Breckenridge, W. H.; Viehland, L. A. Interactions in the B<sup>+</sup>-RG complexes and comparison with Be<sup>+</sup>-RG (RG = He-Rn): evidence for chemical bonding. *J. Phys. Chem. A* **2012**, *116*, 4995–5007.
- <sup>11</sup> Castleman, A. W. Jr.; Keesee, R. G. Clusters: properties and formation. *Ann. Rev. Phys. Chem.* **1986**, *37*, 525–550.

- 
- <sup>12</sup> Walker, N. R.; Walters, R. S.; Duncan, M. A. Frontiers in the infrared spectroscopy of gas phase metal ion complexes. *New J. Chem.* **2005**, *29*, 1495–1503.
- <sup>13</sup> Froudakis, G. E.; Farantos, S. C.; Velegrakis, M. Mass spectra and theoretical modeling of  $\text{Li}^+\text{Ne}_n$ ,  $\text{Li}^+\text{Ar}_n$  and  $\text{Li}^+\text{Kr}_n$  clusters. *Chem. Phys.* **2000**, *258*, 13–20.
- <sup>14</sup> Dhiflaoui, J.; Bouzouita, H.; Berriche, H. Theoretical study of the  $\text{Na}^+\text{Kr}_n$  and  $\text{NaKr}_n$  ( $n=1-25$ ) small clusters. *Phys. Proc.* **2009**, *2*, 1175–1184.
- <sup>15</sup> Prekas, D.; Luder, C.; Velegrakis, M. Structural transitions in metal ion-doped noble gas clusters: experiments and molecular dynamics simulations. *J. Chem. Phys.* **1998**, *108*, 4450–4459.
- <sup>16</sup> El Hadj Rhouma, M. B.; Calvo, F.; Spiegelman, F. Solvation of  $\text{Na}^+$  in Argon Clusters. *J. Phys. Chem. A* **2006**, *110*, 5010–5016.
- <sup>17</sup> Hernández-Rojas, J.; Wales, D. J. Global minima for rare gas clusters containing one alkali metal ion. *J. Chem. Phys.* **2003**, *119*, 7800–7804.
- <sup>18</sup> Fanourgakis, G. S.; Farantos, S. C.; Lüder, Ch.; Velegrakis, M.; Xantheas, S. S. Photofragmentation spectra and potential energy surfaces of  $\text{Sr}^+\text{Ar}_2$ . *Phys. Chem. Chem. Phys.* **1999**, *1*, 977–981.
- <sup>19</sup> Fanourgakis, G. S.; Farantos, S. C.; Potential functions and static and dynamic properties of  $\text{Mg}^{m+}\text{Ar}_n$  ( $m = 1, 2; n = 1-18$ ) clusters. *J. Phys. Chem.* **1996**, *100*, 3900–3909.
- <sup>20</sup> Bauschlicher, C. W. Jr.; Partridge, H.; Langhoff, S. R. Comparison of the bonding between  $\text{ML}^+$  and  $\text{ML}_2^+$  ( $M = \text{metal}, L = \text{noble gas}$ ). *Chem. Phys. Lett.* **1990**, *165*, 272–276.
- <sup>21</sup> Andrejeva, A.; Gardner, A. M.; Graneek, J. B.; Plowright, R. J.; Breckenridge, W. H.; Wright, T. G. Theoretical study of  $\text{M}^+-\text{RG}_2$  ( $\text{M}^+ = \text{Li}, \text{Na}, \text{Be}, \text{Mg}; \text{RG} = \text{He}-\text{Rn}$ ). *J. Phys. Chem. A* **2013**, *117*, 13578–13590.
- <sup>22</sup> Lee, E. P. F.; Wright, T. G. The ionization energy of  $\text{KO}_2(\text{X}^2\text{A}_2)$  and dissociation energies of  $\text{KO}_2$  and  $\text{KO}_2^+$ . *Chem. Phys. Lett.* **2002**, *363*, 139–144.
- <sup>23</sup> Leininger, T.; Nicklass, A.; Küchle, W.; Stoll, H.; Dolg, M.; Bergner, A. The accuracy of the pseudopotential approximation: non-frozen-core effects for spectroscopic constants of alkali fluorides  $\text{XF}$  ( $\text{X} = \text{K}, \text{Rb}, \text{Cs}$ ). *Chem. Phys. Lett.* **1996**, *255*, 274–280.
- <sup>24</sup> Lim, I. S.; Schwerdtfeger, P.; Metz, B.; Stoll, H. All-electron and relativistic pseudopotential studies for the group 1 element polarizabilities from K to element 119. *J. Chem. Phys.* **2005**, *122*, 104103–12.

- 
- <sup>25</sup> Hickling, H. L.; Viehland, L. A.; Shepherd, D. T.; Soldan, P.; Lee, E. P. F.; Wright, T. G. Spectroscopy of  $M^+Rg$  and transport coefficients of  $M^+$  in Rg ( $M = Rb-Fr$ ; Rg = He-Rn). *Phys. Chem. Chem. Phys.* **2004**, *6*, 4233–4239.
- <sup>26</sup> Woon, D. E.; Dunning, T. H. Jr. Gaussian basis sets for use in correlated molecular calculations. IV. Calculation of static electrical response properties. *J. Chem. Phys.* **1994**, *100*, 2975–2988.
- <sup>27</sup> Dunning, T.H. Jr. Gaussian basis sets for use in correlated molecular calculations. I. The atoms boron through neon and hydrogen. *J. Chem. Phys.* **1989**, *90*, 1007–1023.
- <sup>28</sup> Peterson, K. A.; Dunning, T. H. Jr. Accurate correlation consistent basis sets for molecular core–valence correlation effects: the second row atoms Al–Ar, and the first row atoms B–Ne revisited. *J. Chem. Phys.* **2002**, *117*, 10548–10560.
- <sup>29</sup> Nicklass, A.; Dolg, M.; Stoll, H.; Preuss, H. *Ab initio* energy-adjusted pseudopotentials for the noble gases Ne through Xe: Calculation of atomic dipole and quadrupole polarizabilities. *J. Chem. Phys.* **1995**, *102*, 8942–8952.
- <sup>30</sup> Küchle, W.; Dolg, M.; Stoll, H.; Preuss, H. *Ab initio* pseudopotentials for Hg through Rn: I. Parameter sets and atomic calculations. *Mol. Phys.* **1991**, *74*, 1245–1263.
- <sup>31</sup> Peterson, K. A.; Yousaf, K. E. Molecular core-valence correlation effects involving the post-d elements Ga–Rn: Benchmarks and new pseudopotential-based correlation consistent basis sets. *J. Chem. Phys.* **2010**, *133*, 174116–8.
- <sup>32</sup> MOLPRO, version 2012.1, a package of *ab initio* programs, Werner, H.-J.; Knowles, P. J.; Knizia, G.; Manby, F. R.; Schütz, M. *et al.*
- <sup>33</sup> Reed, A. E.; Weinstock, R. B.; Weinhold, F. Natural population analysis. *J. Chem. Phys.* **1985**, *83*, 735–746.
- <sup>34</sup> Bader, R. F. W. *Atoms in Molecules- A Quantum Theory*, Oxford University Press: Oxford, U. K. (1990).
- <sup>35</sup> Mulliken, R. S. Electronic population analysis on LCAO–MO molecular wave functions. I. *J. Chem. Phys.* **1955**, *23*, 1833–1840.
- <sup>36</sup> Keith, T. A.; T. K. Gristmill Software, AIMAll, Overland Park, KS, 2011.
- <sup>37</sup> Frisch, M. J.; Trucks, G. W.; Schlegel, H. B.; Scuseria, G. E.; Robb, M. A.; Cheeseman, J. R.; Scalmani, G.; Barone, V.; Mennucci, B.; Petersson, G. A.; et al. Gaussian 09, Revision D.01; Gaussian, Inc.:Wallingford, CT, 2009.

- 
- <sup>38</sup> Glendening, E. D.; Badenhop, J. K.; Reed, A. E.; Carpenter, J. E.; Bohmann, J. A.; Morales, C. A.; Landis, C. R.; Weinhold, F. NBO 6.0, Theoretical Chemistry Institute, University of Wisconsin, Madison, 2013
- <sup>39</sup> Soldán, P.; Lee, E. P. F.; Wright, T. G. Static dipole polarizabilities ( $\alpha$ ) and static second hyperpolarizabilities ( $\gamma$ ) of the rare gas atoms (He-Rn). *Phys. Chem. Chem. Phys.* **2001**, *3*, 4661–4666.
- <sup>40</sup> Breckenridge, W. H.; Ayles, V. L.; Wright, T. G. Analysis of the bonding in alkali-cation/Rg complexes (Rg = He-Xe) using a simple model potential. *Chem. Phys.* **2007**, *333*, 77–84.
- <sup>41</sup> Lozeille, J.; Winata, E.; Viehland, L. A.; Soldán, P.; Lee, E. P. F.; Wright, T. G. Spectroscopy of  $\text{Li}^+\text{Rg}$  complexes and transport properties of  $\text{Li}^+\text{-Rg}$  (Rg = He-Rn). *Phys. Chem. Chem. Phys.* **2002**, *4*, 3601–3610.
- <sup>42</sup> Andrejeva, A.; Gardner, A. M.; Graneek, J. B.; Breckenridge, W. H.; Wright, T. G. Theoretical study of  $\text{M}^+\text{-RG}_2$ : ( $\text{M}^+ = \text{Ca, Sr, Ba and Ra}$ ;  $\text{RG} = \text{He-Rn}$ ). *J. Phys. Chem. A* **2015**, *119*, 5995–6005.
- <sup>43</sup> Kramida, A.; Ralchenko, Yu.; Reader, J. and NIST ASD Team (2014). NIST Atomic Spectra Database (ver. 5.2), [Online]. National Institute of Standards and Technology, Gaithersburg, MD, USA.
- <sup>44</sup> Cremer, D.; Kraka, E. Chemical bonds without bonding electron density does the difference electron-density analysis suffice for a description of the chemical bond? *Angew. Chem. Int. Ed. Engl.* **1984**, *23*, 627–628.
- <sup>45</sup> Gervasio, G.; Bianchi, R.; Marabello, D. About the topological classification of the metal–metal bond. *Chem. Phys Lett.* **2004**, *387*, 481–484.
- <sup>46</sup> Koritsanszky, T. S.; Coppens, P. Chemical applications of X-ray charge-density analysis. *Chem. Rev.* **2001**, *101*, 1583–1627.
- <sup>47</sup> Harris, J. P.; Dobson, H.; Breckenridge, W. H.; Wright, T. G.  $\text{HM}^+$  and  $\text{HM}^+\text{-He}$  (M = Group 2 metal): Chemical or physical interactions? *J. Chem. Phys.* **2014**, *141*, 094306–9.
- <sup>48</sup> Donchev, A. G. *Ab initio* correlated calculations of rare-gas dimer quadrupoles *Phys. Rev. A* **2007**, *76*, 042713–5
- <sup>49</sup> Stone, A. J. *The Theory of Intermolecular Forces*, Oxford, Clarendon Press, **1996**.
- <sup>50</sup> Stone, A. J. *The Theory of Intermolecular Forces*, Oxford, Oxford University Press, **2013**.